Liquid Crystals
Publication details, including instructions for authors and subscription information:
http://www.informaworld.com/smpp/title~content=t713926090

Statistical model of greyscale in antiferroelectric liquid crystal cells

J. Sabater[a]; J. M. Otón[a]
[a] Dept. Tecnología Fotónica, ETSI Telecomunicación, Ciudad Universitaria, Madrid, Spain

To cite this Article Sabater, J. and Otón, J. M.(1996) 'Statistical model of greyscale in antiferroelectric liquid crystal cells', Liquid Crystals, 21: 2, 175 — 187
To link to this Article: DOI: 10.1080/02678299608032821
URL: http://dx.doi.org/10.1080/02678299608032821

LIQUID CRYSTALS, 1996, VOL. 21, NO. 2, 175–187

Statistical model of greyscale in antiferroelectric liquid crystal cells

by J. SABATER and J. M. OTÓN*
Dept. Tecnología Fotónica, ETSI Telecomunicación, Ciudad Universitaria, E-28040 Madrid, Spain

(*Received 2 October 1995; accepted 28 February 1996*)

Surface stabilized antiferroelectric liquid crystals are known to give multiplex-compatible greyscales by applying simple waveforms. Statistical variations of cell parameters are believed to be at the origin of this greyscale. In this work, an antiferroelectric model is applied to the study of cell statistical variations, aiming to identify the parameters whose variations may account for the experimental results obtained with these cells. It has been found that moderately small parameter variations, well within manufacturing tolerances, may lead to greyscales whose voltage range and shape are similar to those observed experimentally.

1. Introduction

The finding of spontaneous analogue greyscale in surface-stabilized antiferroelectric liquid crystal (AFLC) cells [1] has raised considerable interest, for it opens the possibility of preparing high definition flat panel displays with unlimited colour gamut [2]. The antiferroelectric state is not optically bistable, but AFLCs can be easily stabilized in two opposite ferroelectric states by applying waveforms containing dc bias signals which are compatible with multiplexing [3].

The generation of greyscale in AFLC cells is assigned to statistical variations of cell manufacturing parameters [4]. Microscopic inspection of these cells shows that grey levels are made of small switched and unswitched regions within the pixel area. The AFLC material is assumed to be homogeneous, the variations in switching ranges being assigned to cell surface variations.

In this work, a theoretical model describing the dynamic optical response of AFLC cells has been prepared. The cell surface parameters and the cell thickness have been independently modified. The optical response derived from statistical variations of every parameter has been analysed, and the results have been compared to experimental results. In this way, the parameters that most likely contribute to greyscale formation have been identified.

Cell surfaces are characterized by a surface energy and a molecular pretilt. No asymmetries between surfaces have been introduced; a symmetric energy expression is used also. These parameters and the cell thickness have been allowed to vary while applying some of the waveforms proposed for greyscales in the literature [5]. In this way, the dynamic behaviour of an inhomogeneous cell has been studied.

2. Homogeneous model

2.1. Geometry

A bookshelf cell structure is assumed. Actual AFLC cells would probably adopt chevron structures; nevertheless, this feature does not directly affect the greyscale and complicates the formulation. The coordinate system employed for the formulation is shown in figure 1. Two layers, labelled with an i sub-index, are taken; this is

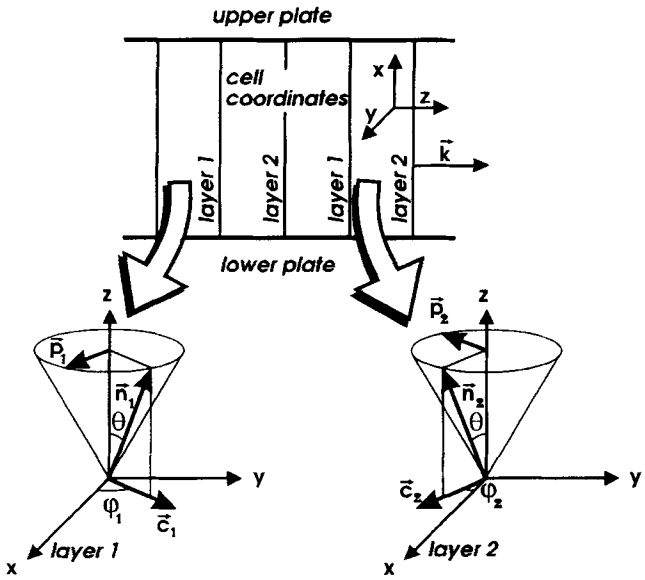

Figure 1. System geometry.

*Author for correspondence.

0267–8292/96 $12·00

necessary for considering the characteristic layer coupling shown by AFLCs [6]. Other models include more layers to account for long distance interactions; again, this complicates the model and does not directly affect the greyscale mechanism.

The problem formulation requires three unit vectors. Two of them are different for each layer:

- $\mathbf{k}$ perpendicular to the smectic layers
- $\mathbf{c}_i$ projection of the molecular director on each smectic layer
- $\mathbf{p}_i$ parallel to the spontaneous polarization in each layer.

The expressions of these three vectors are:

$$\mathbf{k} = [0, 0, 1] \tag{1}$$

$$\mathbf{c}_i = [\cos\varphi_i, \sin\varphi_i, 0] \tag{2}$$

$$\mathbf{p}_i = [-\sin\varphi_i, \cos\varphi_i, 0] \tag{3}$$

where φ_1 and φ_2 are the azimuthal angles of the molecular director in each layer.

2.2. *System energy*

The system energy is made of several terms that are separately described below.

2.2.1. *Antiferroelectric coupling*

Describes the coupling between adjacent layers. In the AFLC case, the molecules of adjacent layers tend to orient opposite to each other. A formulation of this energy is [6]:

$$f_c = \alpha \mathbf{P}_1 \cdot \mathbf{P}_2 = \frac{1}{4}\alpha P_s^2 \cos(\varphi_2 - \varphi_1) \tag{4}$$

where α is a coupling constant, negative in AFLCs and positive in ferroelectrics. P_s is the spontaneous polarization of the antiferroelectric material.

2.2.2. *Elastic energy*

A simple expression will be used for this energy. Its formulation is:

$$f_{elas} = \frac{B}{4}\sum_{i=1}^{2}[(\mathbf{k}\cdot\nabla\times\mathbf{c}_i)^2 + (\nabla\cdot\mathbf{c}_i)^2]$$

$$= \frac{B}{4}[\varphi_{1,y}^2 + \varphi_{2,y}^2] \tag{5}$$

where B is a generic elastic energy constant of the material.

2.2.3. *Electric energy*

This energy includes the interactions of the applied field with the spontaneous polarization and the dielectric tensor:

$$f_{elec} = -\frac{P_s}{2}\sum_{i=1}^{2}\cos\varphi_i \frac{V}{d} - \frac{\varepsilon_1 + \delta\varepsilon}{4}\left(\frac{V}{d}\right)^2 \times \left(2 + \sum_{i=1}^{2}\frac{(\Delta\varepsilon\sin^2\theta - \delta\varepsilon)\sin^2\varphi_i}{\varepsilon_1 + \delta\varepsilon}\right) \tag{6}$$

In this expression, V stands for the external applied voltage, d for the cell width, P_s for the material's spontaneous polarization, ε_1 for the dielectric permittivity, $\Delta\varepsilon$ for the dielectric anisotropy, $\delta\varepsilon$ for the dielectric biaxiality and θ for the molecular tilt.

2.2.4. *Surface energy*

A symmetric energy expression is used. It is defined by its magnitude g and the pretilt β. Two equivalent expressions are obtained for the upper (up) and lower (dn) plate:

$$f_{up,i} = g_{up}(\sin\theta\sin\varphi_i - \sin\beta_{up})^2 \tag{7}$$

$$f_{dn,i} = g_{dn}(\sin\theta\sin\varphi_i - \sin\beta_{dn})^2 \tag{8}$$

2.3. *Problem formulation*

The evolution of the different system energies can be described by a set of Ginzberg–Landau differential equations. Their general expression is:

$$\lambda\frac{\partial\varphi_i}{\partial y} = -\frac{\partial f}{\partial\varphi_i} + \frac{\partial}{\partial y}\frac{\partial f}{\partial\varphi_{i,y}} \tag{9}$$

where λ is the rotational viscosity of the material.

Applying these equations to φ_1 and φ_2, the following expressions are obtained:

$$\lambda\varphi_{1,t} = \frac{1}{4}\left[-\alpha P_s^2\sin(\varphi_2 - \varphi_1) - 2P_s\frac{V}{d}\sin\varphi_1 + \left(\frac{V}{d}\right)^2(\Delta\varepsilon\sin^2\theta - \delta\varepsilon)\sin 2\varphi_1\right] + \frac{B}{2}\varphi_{1,yy} \tag{10}$$

$$\lambda\varphi_{2,t} = \frac{1}{4}\left[-\alpha P_s^2\sin(\varphi_1 - \varphi_2) - 2P_s\frac{V}{d}\sin\varphi_2 + \left(\frac{V}{d}\right)^2(\Delta\varepsilon\sin^2\theta - \delta\varepsilon)\sin 2\varphi_2\right] + \frac{B}{2}\varphi_{2,yy} \tag{11}$$

It is useful to normalize the y coordinate to the cell thickness d, and time to $\lambda d^2/B$. The normalized dynamic

equations have the following form:

$$\kappa = \frac{y}{d} \tag{12}$$

$$\zeta = \frac{t}{\left(\frac{\lambda d^2}{B}\right)} \tag{13}$$

$$\varphi_{1,\zeta} = \frac{d^2}{4B}\left[-\alpha P_s^2 \sin(\varphi_2 - \varphi_1) - 2P_s \frac{V}{d} \sin\varphi_1 + \left(\frac{V}{d}\right)^2 (\Delta\varepsilon \sin^2\theta - \delta\varepsilon) \sin 2\varphi_1 \right] + \frac{1}{2}\varphi_{1,\kappa\kappa} \tag{14}$$

$$\varphi_{2,\zeta} = \frac{d^2}{4B}\left[-\alpha P_s^2 \sin(\varphi_1 - \varphi_2) - 2P_s \frac{V}{d} \sin\varphi_2 + \left(\frac{V}{d}\right)^2 (\Delta\varepsilon \sin^2\theta - \delta\varepsilon) \sin 2\varphi_2 \right] + \frac{1}{2}\varphi_{2,\kappa\kappa} \tag{15}$$

Boundary conditions for these equations are derived from the surface energy and the volume energy:

$$\frac{B}{2} \left.\frac{\partial\varphi_i}{\partial y}\right|_{y=d} - 2g_{up}(\sin\theta \sin\varphi_i|_{y=d} - \sin\beta_{up}) \times \sin\theta \cos\varphi_i|_{y=d} = 0 \tag{16}$$

$$\frac{B}{2} \left.\frac{\partial\varphi_i}{\partial y}\right|_{y=0} + 2g_{dn}(\sin\theta \sin\varphi_i|_{y=0} - \sin\beta_{dn}) \times \sin\theta \cos\varphi_i|_{y=0} = 0 \tag{17}$$

After normalization, the following expression is obtained:

$$\frac{B}{2d} \left.\frac{\partial\varphi_i}{\partial\kappa}\right|_{\kappa=1} 2g_{up}(\sin\theta \sin\varphi_i|_{\kappa=1} - \sin\beta_{up}) \times \sin\theta \cos\varphi_i|_{\kappa=1} = 0 \tag{18}$$

$$\frac{B}{2d} \left.\frac{\partial\varphi_i}{\partial\kappa}\right|_{\kappa=0} + 2g_{dn}(\sin\theta \sin\varphi_i|_{\kappa=0} - \sin\beta_{dn}) \times \sin\theta \cos\varphi_i|_{\kappa=0} = 0 \tag{19}$$

2.4. *Default values of the parameters*

A set of default values has been chosen as a starting point for the simulations. The tilt angle and the spontaneous polarization of the antiferroelectric mixture CS-4000 (Chisso) are used. The range of other values is the same as used in the case of ferroelectric mixtures. The compression modulus range is determined by its relative weight in the expressions. If α is too large, its term overcomes the remaining terms; if α is too small, its effect is negligible. Both situations contradict experimental results. The value used here is similar to others employed in the literature [6]:

* $d = 2\,\mu m$
* $\theta = 27{\cdot}1^\circ$
* $\alpha = 1{\cdot}25 \times 10^{10}\,Nm^3\,C^{-2}$
* $B = 5 \times 10^{-9}\,N$
* $\Delta\varepsilon = -0{\cdot}9\varepsilon_0$
* $\delta\varepsilon = 0{\cdot}5\varepsilon_0$
* $g_{up} = g_{dn} = 5 \times 10^{-3}\,Nm^{-1}$
* $P_s = 79{\cdot}8\,nC\,cm^{-2}$
* $\varepsilon_l = 5\varepsilon_0$
* $\beta_{up} = \beta_{dn} = 3^\circ$
* $\lambda = 150 \times 10^{-3}\,Ns\,m^{-1}$

2.5. *Waveforms*

Waveforms employed in multiplexed AFLC greyscale generation [5] can be grouped in two families, depending on the function of the selection pulse: (i) the pulse produces a (partial) AFLC→FLC switching, which is eventually stabilized by a bias signal, and (ii) the sample is first fully switched to the FLC phase, and the selection pulse is used for allowing partial relaxation of the FLC phase back to the AFLC phase. Again, the resulting configuration is stabilized by a bias signal. Note that both addressing waveform families require to start from a known configuration: relaxed AFLC in the first case, and electrically induced FLC phase in the second case.

Figure 2 shows two waveforms that belong to the first and second family, respectively. These have been chosen as test waveforms in this work. The first waveform, figure 2(*a*), besides the selection pulse and the bias voltage, includes a reset time long enough for achieving full relaxation to the AFLC phase regardless of the previous state of the pixel. Otherwise (i.e. if reset is too short), the effect of the selection pulse depends on the pixel history. This reset strategy is not the best (for actual reset times may be comparable to frame time) but it is the simplest none the less, which is convenient for testing the model.

The second waveform, figure 2(*b*), does not require reset, as the known configuration previous to the selection pulse is achieved by a saturating prepulse that entirely switches the pixel to the FLC state. In this case, the selection pulse merely modulates the relaxation time of the pixel. Non-relaxed areas after selection are kept in the FLC state by the bias voltage.

3. Statistical model

3.1. *Introduction*

Given the statistical nature of AFLC grey levels, a non-homogeneous model of pixel behaviour with external electric signals was assumed. In this model, the pixel area is characterized by a statistical distribution which determines the percentage of the area whose phase is changed by the electric signal, either switching from

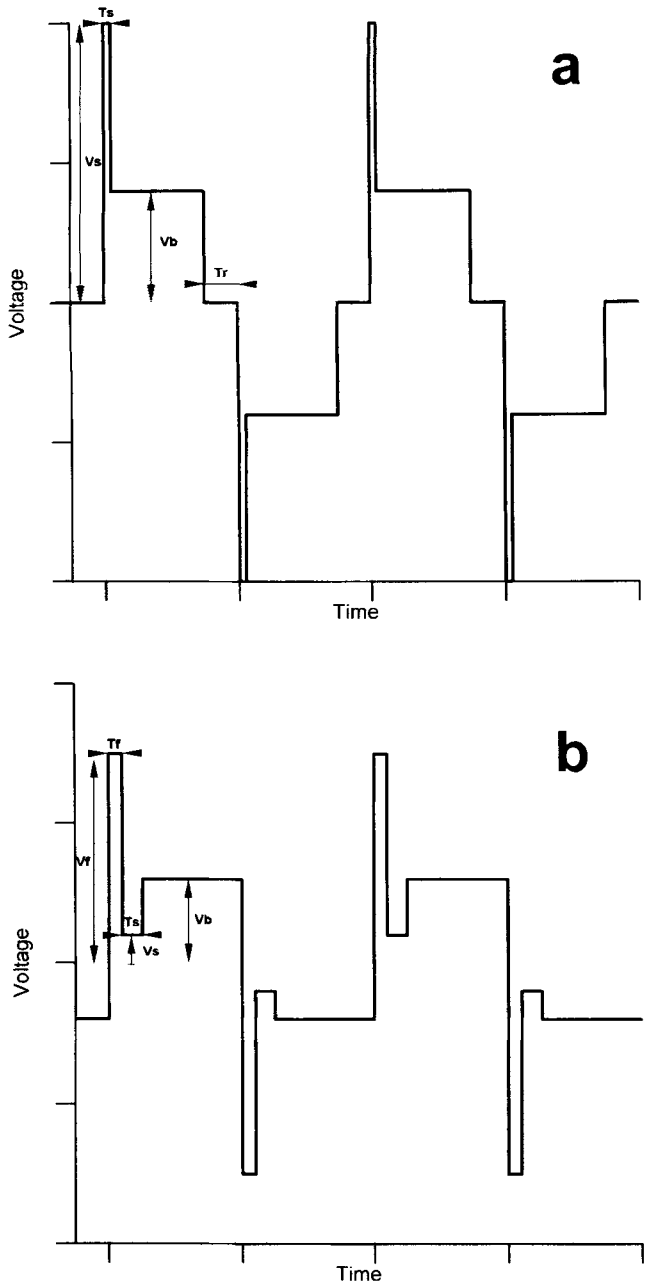

Figure 2. Definition of two waveform families capable of greyscale driving. The first (*a*) is based on a transition from antiferroelectric to ferroelectric, whereas the second (*b*) is based on the opposite transition.

AFLC to FLC, or relaxing from FLC to AFLC. The distribution function can be formalized as follows:

$$\Upsilon = \Upsilon(\xi, \chi) \tag{20}$$

where ξ is a vector including the waveform parameters affecting the phase changes. In the above waveforms, these are: selection voltage (V_s), selection pulse duration (t_s), bias voltage (V_b).

Reset time (t_r) in the first waveform is assumed to be large enough for complete relaxation to the AFLC phase. It follows that, above a certain threshold, t_r does not affect switching distributions. V_f and t_f in the prepulse of the second waveform are assumed to be sufficient to achieve full phase transition to FLC regardless of the previous pixel state. Therefore, these do not affect the distributions either. In these conditions, ξ is a tridimensional vector:

$$\xi = (V_s, t_s, V_b) \tag{21}$$

Vector χ includes all the cell parameters affecting switching. These parameters can be split into two groups, related to the material itself (ω) and the manufacturing process (τ), respectively. It is reasonable to assume that the liquid crystal material is the same throughout the cell; therefore material parameters should be discrete values (i.e. with no distribution). Manufacturing parameters, on the other hand, may be different in different points of the cell, thus requiring a statistical distribution for their description. These parameters mainly concern cell thickness and surface conditioning. These features are the result of several fabrication steps, and may be related to each other. In this work, however, manufacturing parameters are considered independent for simplicity. Parameters are characterized by their mean and standard deviation. Two distributions, normal and uniform, are tested to assess their effect on the greyscale shape. The general form of vector χ is:

$$\chi = (\chi_1, \chi_2, \ldots, \chi_N, \chi_{N+1}, \ldots, \chi_{M-1}, \chi_M) = (\tau, \omega)$$

where

$$\tau = [\chi_1(\overline{\chi_1}, \sigma_{\chi_1}) \ldots \chi_N(\overline{\chi_N}, \sigma_{\chi_N})] \rightarrow \text{Manufacturing}$$

and

$$\omega = (\chi_{N+1} \cdots \chi_M) \rightarrow \text{Material} \tag{22}$$

In this case, $N = 3$; the elements of τ are: surface energy (γ), surface pretilt (β), and cell thickness (d). The elements of ω are the remaining model parameters, which characterize the AFLC material.

If the cell were homogeneous, i.e. $\sigma_\gamma = \sigma_\beta = \sigma_d = 0$, then the function Υ would have only two values, 0% and 100%. This would define two areas separated by a multidimensional surface. If vector χ is known, this surface can be described by a function:

$$\Omega(\xi) = \Omega(V_s, t_s, V_b) = 0 \tag{23}$$

This implicit expression can be made explicit by taking t_s as a function of V_s and V_b, as the projection of Ω onto the V_s–V_b plane is single-valued, i.e. given these two voltages, a single solution (if any) for minimum switching t_s is found. The resulting surface may be considered a generalized V–t surface. It should be noted, however,

that its shape depends on the material and on the applied waveform.

3.2. *Generalized V–t surfaces*

Figure 3 (*a*) shows the theoretical *V–t* surface corresponding to an arbitrary homogeneous cell when the first waveform is applied. Figure 3 (*b*) depicts the same cell with the second waveform. Figures 3 (*a*) and 3 (*b*) actually show only the intermediate part of their complete graphs. These surfaces have three different zones corresponding to three ranges of V_b values. Indeed, if V_b is below a certain threshold, V_{th1}, the cell always relaxes to the AFLC phase, regardless of the previous voltage signals applied to the pixel. In other words, V_b is too low to stabilize the FLC phase. On the other hand, if V_b is above a certain threshold, V_{th2}, the cell switches to the FLC phase, for the AFLC phase is not stable for this voltage:

$$V_b < V_{th1} \Rightarrow t_s \to \infty \quad V_b > V_{th2} \Rightarrow t_s = 0 \qquad (24)$$

These generalized *V–t* curves can be used for selecting the best working point for greyscale generation. This is done in the next sections for the two waveforms used in this work.

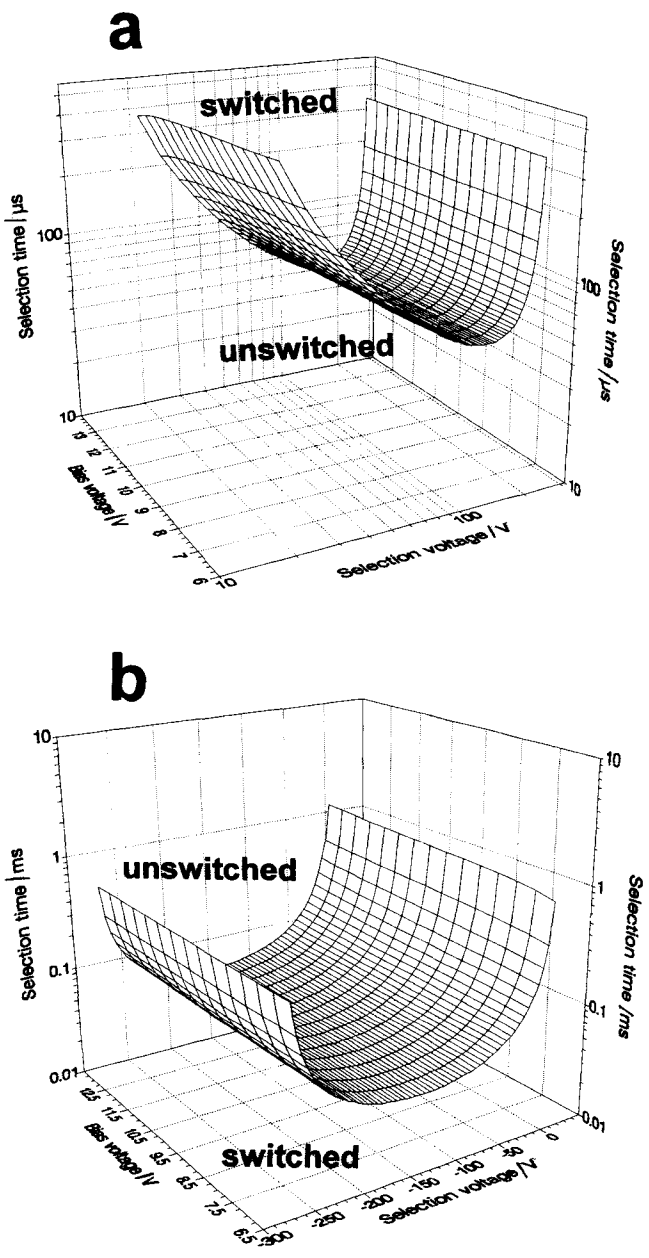

Figure 3. Generalized *V–t* curves corresponding to the first (*a*) and the second (*b*) waveform families.

3.2.1. *Working point selection: first waveform*

3.2.1.1. *Minimum switching time.* In the intermediate V_b range mentioned above, the surface sections for constant V_b are similar to typical *V–t* curves found in FLCs. The minimum is due, as in the FLC case, to the decrease of the effective torque experienced by the molecule as the relative weight of the dielectric term increases with voltage. No remarkable differences of minimum t_s are found within the allowed limits of V_b. Therefore, no selection criteria for best working point (concerning V_b) can be derived from this feature; other system characteristics must be used for selecting the best set of parameters.

3.2.1.2. *Contrast.* Computing the transmission at normal incidence of stabilized AFLC and FLC phases as a function of bias voltage (figure 4 (*a*)), an increase of transmission in both dark and clear states is found as V_b increases. As expected, two regions can be observed. In the first region the transmission of the clear (FLC) state increases and eventually stabilizes; in the second, the transmission of the dark (AFLC) state abruptly increases. The maximum contrast (figure 4 (*b*)) is in the intermediate area. This criterion points to a moderately high V_b. No information on the best values of V_s and t_s is obtained from contrast.

3.2.1.3. *Relaxation time.* Relaxation time may be important for multiplexed displays, as it has an influence on flickering and other features (e.g. integrated brightness and contrast) affecting the final appearance of the display. What ultimately matters, in this context, is not the physical relaxation of the system, but the time that elapses until stabilization of the optical transmission. The calculation of this time requires the computation of T_{ON} and T_{OFF} transmissions of the clear and dark states, respectively. The relaxation time is defined as the time elapsed from the end of the selection pulse to the

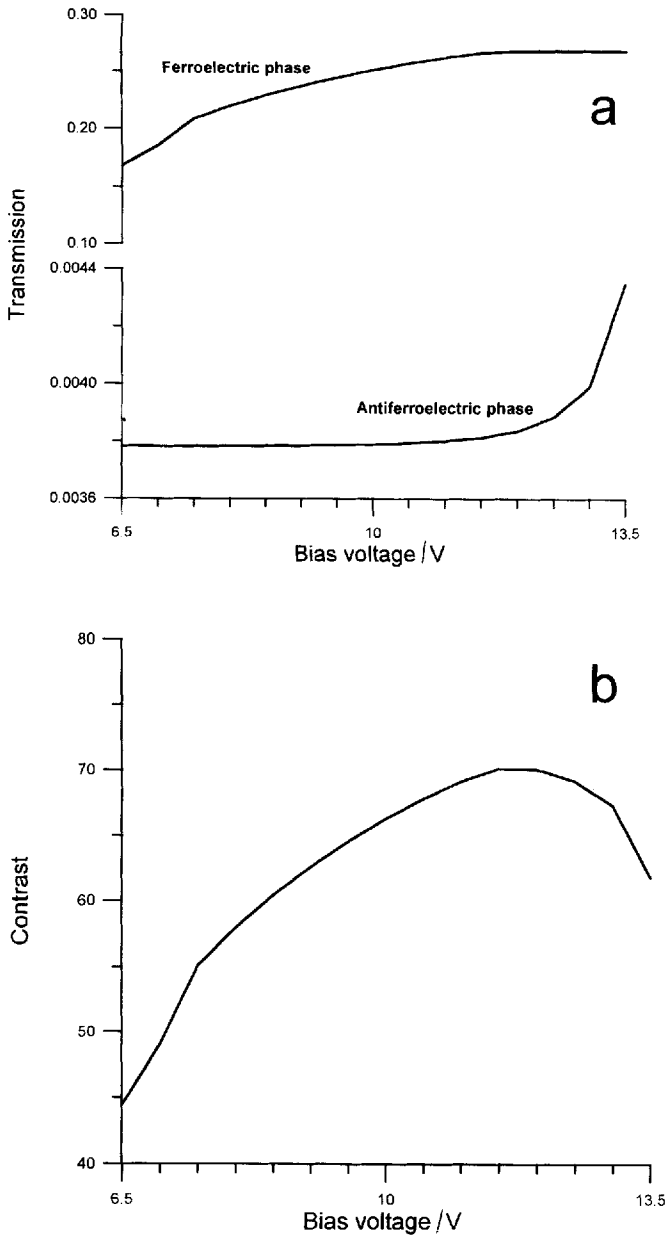

Figure 4. (*a*) Optical transmission of the ferroelectric and antiferroelectric states as a function of the bias voltage; (*b*) contrast between the ferroelectric and the antiferroelectric states as a function of bias voltage.

following condition:

$$\frac{T - T_{ON}}{T_{ON} - T_{OFF}} < 0{\cdot}1 \quad \text{or} \quad \frac{T - T_{OFF}}{T_{ON} - T_{OFF}} < 0{\cdot}1 \qquad (25)$$

where T is the current pixel transmission. It is not possible to use simply the points 90% and 10% of T_{ON}, because low values of V_b would give small transmissions; then the transmission immediately after the selection pulse could be higher than the stable value of T_{ON}. In such a case, the employed criterion would correctly

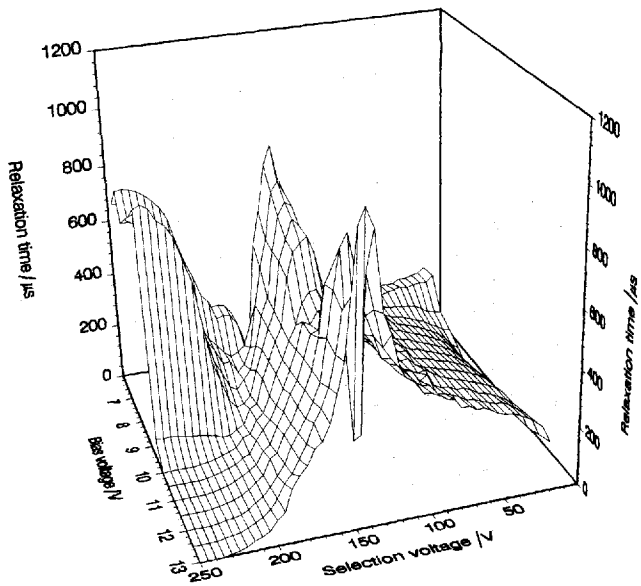

Figure 5. Relaxation time of the first waveform.

compute the time required for stabilization of the transmission, whereas the 90%–10% criterion would give zero. The mean stabilization time has been calculated as the average of the stabilization times corresponding to 40 working points near every point of the V–t surface shown in figure 4. In these 40 points, V_b and t_s are kept constant, and V_s is varied. Figure 5 shows the mean stabilization time for every point of figure 3 (*a*). Two regions with exceedingly high times are found: one is a band of V_s values, independent of the value of V_b. The other is the region of high V_s and low V_b. The first region matches the area of minimum selection time; relaxation in this region is slow because the final switching is partially achieved by the bias voltage. The reason for the long time in the second region is different: here the selection pulse entirely switches the pixel, and the resulting transmission is well above the transmission level stabilized by the low bias voltage. A fairly large time is then required for reducing transmission to the stabilized level.

3.2.1.4. *Overall stabilization time.* Figure 5 is misleading, because relaxation time is computed only from the end of the selection pulse. Figure 6 shows the sum of the selection and relaxation times, i.e. the sum of curves shown in figures 3 (*a*) and 5. This may be considered as the time required for achieving a certain grey level. Comparing figures 5 and 6, a change in the orientation of the surface borders can be seen. Moreover, two regions having minimum overall time are found. The fastest results are given by a high selection/moderate bias voltage. This region, however, may be outside practical use, for two reasons: one is that the high

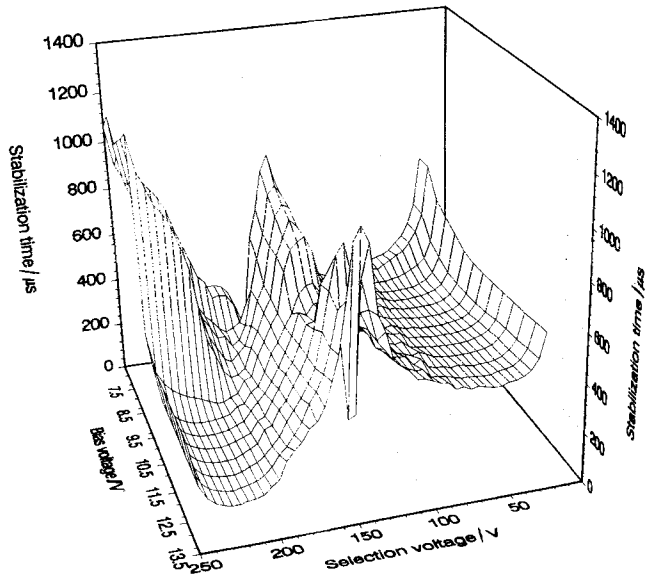

Figure 6. Stabilization time of the first waveform.

voltage required in selection may be beyond the usual electronics employed in addressing. A second, more subtle, reason is that second order effects, not included in the model, may be relevant at high voltage.

The second region is located at low selection/moderate bias voltage. A further advantage of this region is that the area is quite flat, allowing some tolerance in the selection of the working point; this may be useful, if the actual working point ought to meet other criteria (e.g. related to multiplexing rate or frame time). A minimum is located in the moderate–high bias voltage region. From this point, the time increases faster towards smaller V_b values.

3.2.1.5. *Bias voltage limits.* Another criterion for selection of the working point is dictated by practical limits in bias voltage. If the cell is designed for multiplexed addressing, the actual voltage perceived by every pixel during the bias is not the bias voltage alone, since data voltage for the remaining rows are also applied along the frame time. As V_b is bounded by an upper and a lower threshold, the selected V_b must be far enough from these limits to avoid the thresholds in the worse case. For example, if data amplitude is $\pm V_d$, the selected bias voltage must be within $V_{th1} + V_d$ and $V_{th2} - V_d$.

In conclusion, the best set of parameters for this waveform includes a moderately high V_b, below the limit $V_{th2}-V_d$, and a moderately high V_s.

3.2.2. *Working point selection: second waveform*

3.2.2.1. *General remarks.* Figure 3(*b*) shows the *V–t* surface of the second waveform. The intersections for constant V_b are similar to those obtained in the previous waveform. However, their meaning is different. *V–t* surfaces separate spatial switching and non-switching regions. In the first waveform, the switching region is located above the surface; in this waveform, the switching region is below. The reason is that the selection voltage plays a different role in each case.

In the first waveform, the selection pulse switches from AFLC to FLC phase; for low voltage, the switching time is inversely proportional to the modulus of the selection voltage. For higher voltage, the weight of the dielectric term changes the trend. In the second waveform, the selection voltage seeks to speed up the relaxation from FLC to AFLC phase, as the pixel has been completely switched to the FLC phase in advance. Let us consider, for example, a positive switching prepulse (V_f, t_f) leaving the cell in the FLC UP state. The selection voltage must be lower than any bias voltage able to stabilize the FLC phase; otherwise, no relaxation is obtained for any selection time. If a positive selection voltage, between zero and this upper limit, is chosen, relaxation is produced *against* the selection pulse (i.e. the effect of the selection pulse would be to decrease the effective repulsion between parallel molecules located in adjacent layers, thus favouring the FLC state stability). Negative selection voltages decrease the relaxation time by moving the molecules in the layers from the switched position to an intermediate one, from which relaxation is faster. If the selection pulse is reduced further (larger negative values), direct switching from FLC UP state to FLC DN state is obtained; in this case, the relaxation time is similar to the value with no applied field. Even larger negative selection pulses cancel out any switching or relaxation, since the dielectric term hinders modifications in the position of the molecules.

3.2.2.2. *Selection criteria.* The selection of the working point will use the same criteria as in the previous case. These are summarized below.

The optimization of contrast is determined by the applied bias voltage; no differences exist between waveforms. A moderately high V_b value is required.

Relaxation time has been evaluated with the same premises as in the previous case. Figure 7 shows the mean relaxation time corresponding to every point of the *V–t* surface shown in figure 3(*b*). There is a central region having high values (similar to figure 8) and two areas where the time is zero, one for high V_b and high V_s and another for high V_b and low V_s. For medium values of V_s, a plateau with moderate stabilization times can also be seen.

The overall (selection + relaxation) stabilization time is shown in figure 8. This is the sum of figures 3(*b*) and 7. Comparing with figure 7, the fast response area for high V_b and low V_s is further reduced, and the plateau region

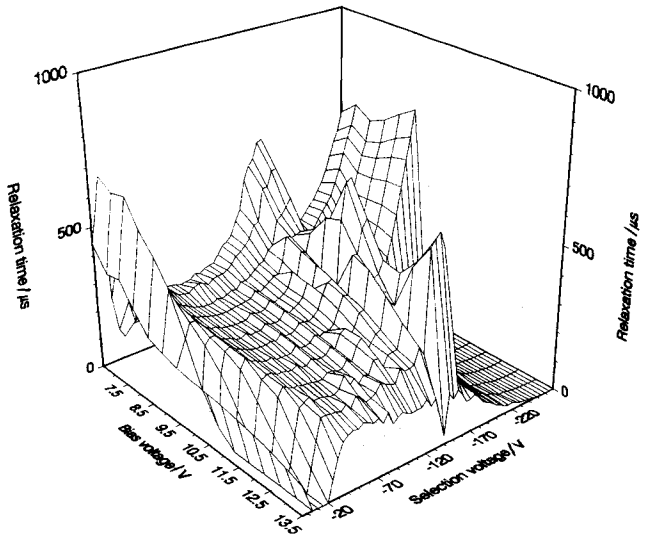

Figure 7. Relaxation time of the second waveform.

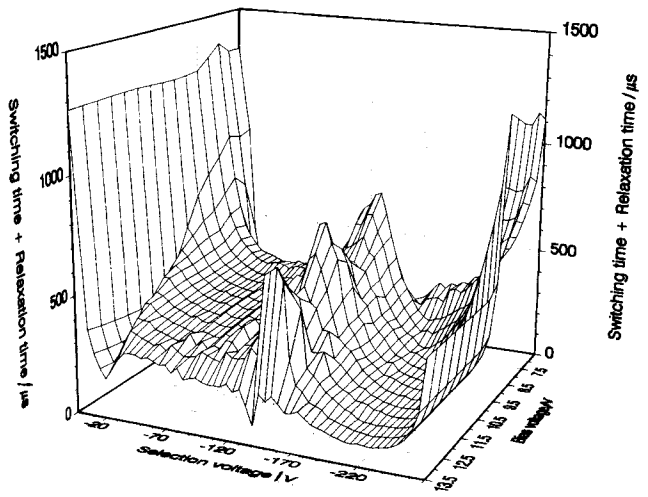

Figure 8. Stabilization time of the second waveform.

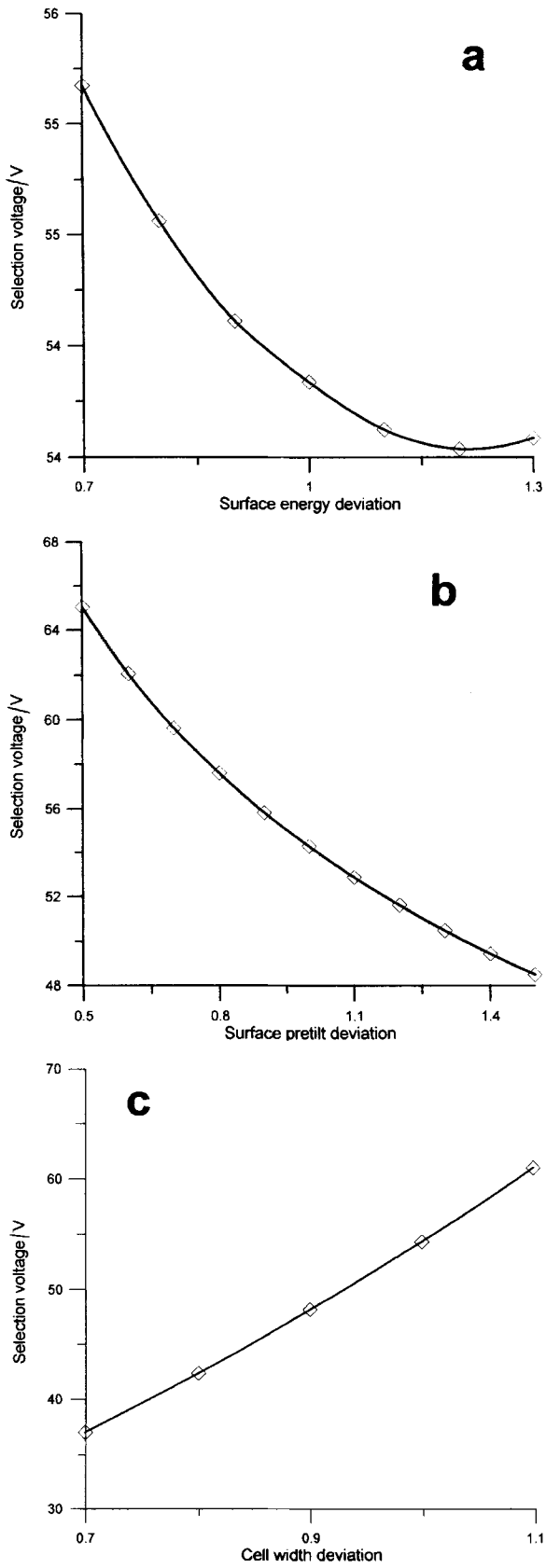

Figure 9. Minimum switching time for the first waveform as a function of normalized: (*a*) surface energy, (*b*) surface pretilt, and (*c*) cell width.

is relatively unaltered. The best results, obtained in the high V_s area, are probably useless for the same reasons pointed out above.

The limits imposed by the bias voltage are the same as in the previous case.

In conclusion, the best set of parameters for this waveform includes a moderately high V_b. Two possible ranges, low and medium, of V_s can be used. The choice depends on the required tolerance to small variations of the applied wave.

3.3. *Statistical variation of parameters*

Once the working point is chosen, the effect of distributed populations of manufacturing parameters on greyscale generation can be assessed. As mentioned above, each parameter will be defined by a mean value and a standard deviation; values are chosen as the values employed on the V–t surfaces for both waveforms and null. This selection seems reasonable, at least for low/moderate values of standard deviation.

Plotting the function Υ of equation (20) requires $4 + N$ dimensions: 3 for the elements of ξ (equation (21)), N for the values of σ_γ, σ_β, and σ_d (equation (22)), and one for the function itself. Sections of this plot in 3-D graphs have been obtained by fixing t_s and V_b and assuming that only one parameter is distributed. These sections, therefore, show the percentage of switched pixel as a function of V_s while one manufacturing parameter is distributed according to its standard deviation. These constraints implicitly assume that the distributions of parameters are independent of each other.

The problem is now reduced to the evaluation of the fraction of switched pixel for a given selection voltage, with known V_b and t_s. Every point of the pixel will have its own V–t surface corresponding to the specific value of the varying parameter χ_i at that point. Therefore, the relationship between the possible values of χ_i and the minimum switching voltage must be established. Once this is known, the fraction of switched pixel can be derived from the distribution function of χ_i.

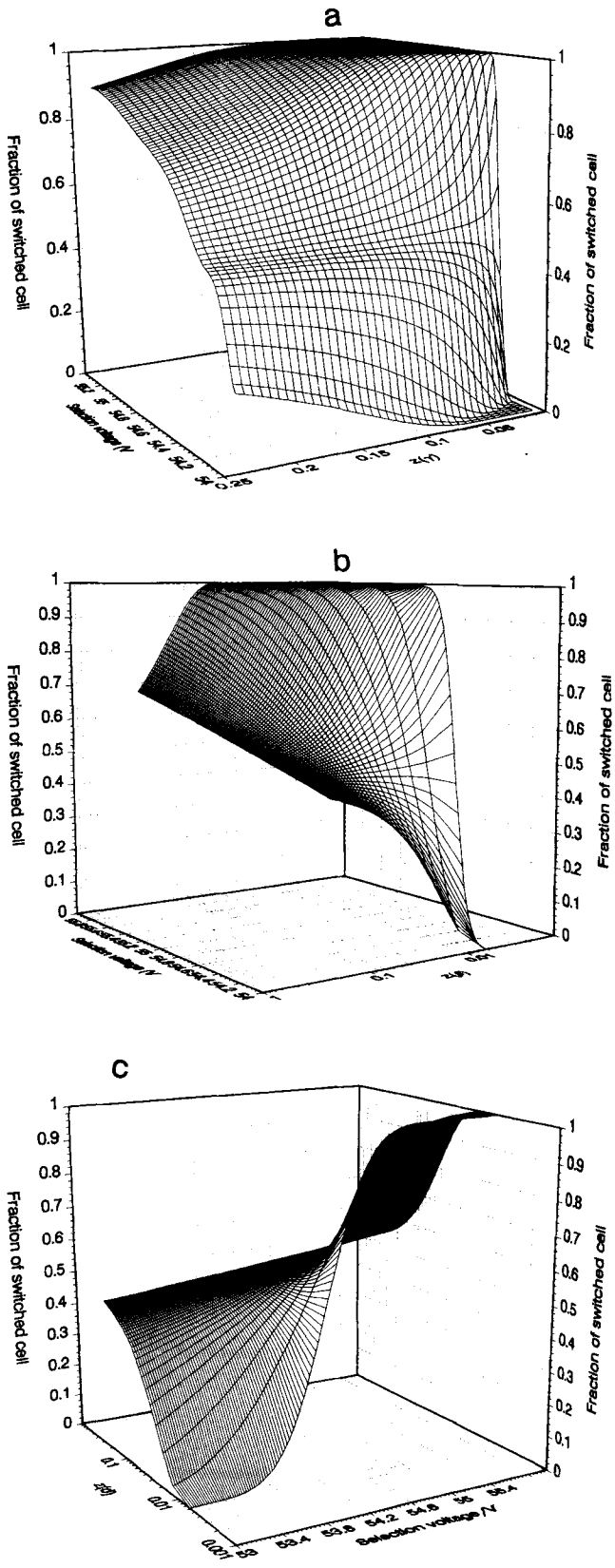

Figure 10. Fraction of switched cell as a function of selection voltage and variation of the distributed parameter. (*a*) corresponds to surface energy variation, where $z(\gamma)$ stands for the standard deviation of the surface energy divided by the surface energy mean value; (*b*) to surface pretilt variation, where $z(\beta)$ stands for the standard deviation of the surface pretilt divided by the surface pretilt mean value; (*c*) to cell width variation, where $z(d)$ stands for the standard deviation of the cell width divided by the cell width mean value. The parameter is assumed to be normally distributed.

The relationship between χ_i and minimum switching voltage was obtained as follows: V–t surfaces corresponding to 10 different χ_i values about the mean χ_i were evaluated. A spline interpolation was used to approximate the value of V_s for every tuple of V_b, t_s, and χ_i. These interpolated V_s values were applied to a second spline interpolation to calculate the selection voltage corresponding to any arbitrary χ_i.

Figures 9(*a*), 9(*b*) and 9(*c*) show the variations of selection voltage for a distributed surface energy, pretilt, and cell thickness, respectively, using the first waveform. A similar set has been obtained for the second waveform. The remaining results have been obtained for both waveforms. Although working points are different in each case, the curve shapes are quite similar; therefore the figures of the second waveform are omitted.

Surface energy variations, as seen in the figures, have smaller influence on the selection voltage than pretilt or cell thickness. It should be noted, however, that pretilt and surface energy are considered independent of each other for simplicity; these two parameters are usually linked in liquid crystal models. Pretilt deviations, moreover, are taken as angle fractions; this obviously depends on the origin chosen for the measured angle. In low pretilt cells, like those employed here, an angle increment of 1° corresponds to a substantial percentage variation of the pretilt.

3.4. *Switched pixel fraction*

Figures 10(*a*), 10(*b*) and 10(*c*) show the fraction of switched pixel as a function of the selection voltage for different values of the standard deviation of surface energy, pretilt and cell thickness, respectively. Gaussian distributions are assumed, and the first waveform is used. The values of t_s and V_b are fixed to 100 µs and 12 V, respectively. Figures 11(*a*), 11(*b*) and 11(*c*) show the same graphs using uniform distributions. Comparing the results for both distributions with experimental greyscales obtained in real cells, the gaussian distribution yields more realistic results. In the remaining sections, only the results corresponding to gaussian distributions are shown.

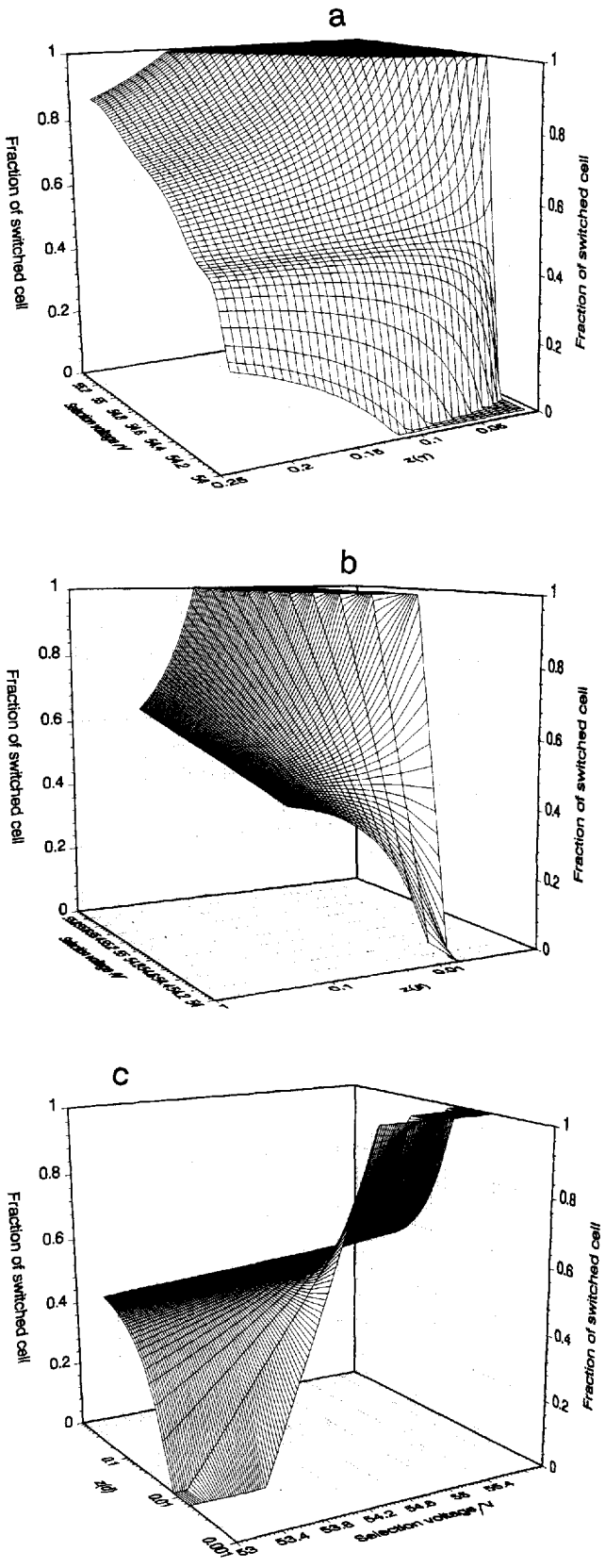

Figure 11. Fraction of switched cell as a function of selection voltage and variation of the distributed parameter. (*a*), (*b*) and (*c*) are the same as in figure 10 and its caption. The parameter is assumed to be uniformly distributed.

4. Greyscales

4.1. *Optical transmission of partially switched pixels*

Given a partially switched pixel, the optical transmission is not exactly proportional to the fraction of switched area. Optical transmission is calculated as:

$$T(V) = \int_{-\infty}^{\chi(V)} p(\chi) T_{\mathrm{OFF}}(V, \chi)\, \mathrm{d}\chi + \int_{\chi(V)}^{\infty} p(\chi) T_{\mathrm{ON}}(V, \chi)\, \mathrm{d}\chi \tag{26}$$

where $T(V)$ is the transmission at a voltage V, $\chi(V)$ is the maximum non-switching value of the distributed parameter for voltage V, $T_{\mathrm{OFF}}(V, \chi)$ is the transmission of a uniform AFLC cell corresponding to the parameter χ and voltage V, and $p(\chi)$ is the probability associated with the value χ of the distributed parameter. Figures 12(*a*), 12(*b*) and 12(*c*) show the function $T_{\mathrm{OFF}}(V, \chi)$ and $T_{\mathrm{ON}}(V, \chi)$ for the three parameters, surface energy, pretilt, and cell thickness. The function $T(V)$ has also been computed including the effect of the different stable transmissions along the cell derived from spatial distributions of manufacturing parameters. No significant differences, at least for moderate σ_χ values, have been found between this function and the fraction of switched cell. Therefore, the previous graphs, where switched fractions were shown, may be accurately taken as transmission curves.

4.2. *Greyscale voltage range*

A practical analogue greyscale for multiplexed AFLC displays requires a fairly specific greyscale voltage range. If the voltage range is too small, small external variations (e.g. room temperature) may have a dramatic effect on the greyscale. If it is too large, data signals may substantially modify the bias voltage of other rows, producing unwanted changes in pixel transmission along the frame time, and inducing crosstalk and flickering. The model developed in this work may be used for predicting the voltage range required for the greyscale to arise under a given set of parameters. For example, figure 13 shows the voltage range needed for varying the pixel transmission from 10% to 90%, using the first waveform, as a function of bias voltage and switching time, i.e. the two variables that were kept constant in previous sections. In these figures, $\sigma_\gamma = \sigma_\beta = \sigma_d = 3{\cdot}5\%$ of the mean value of the parameter. These voltage range surfaces can be used as supplementary criteria for working point selection.

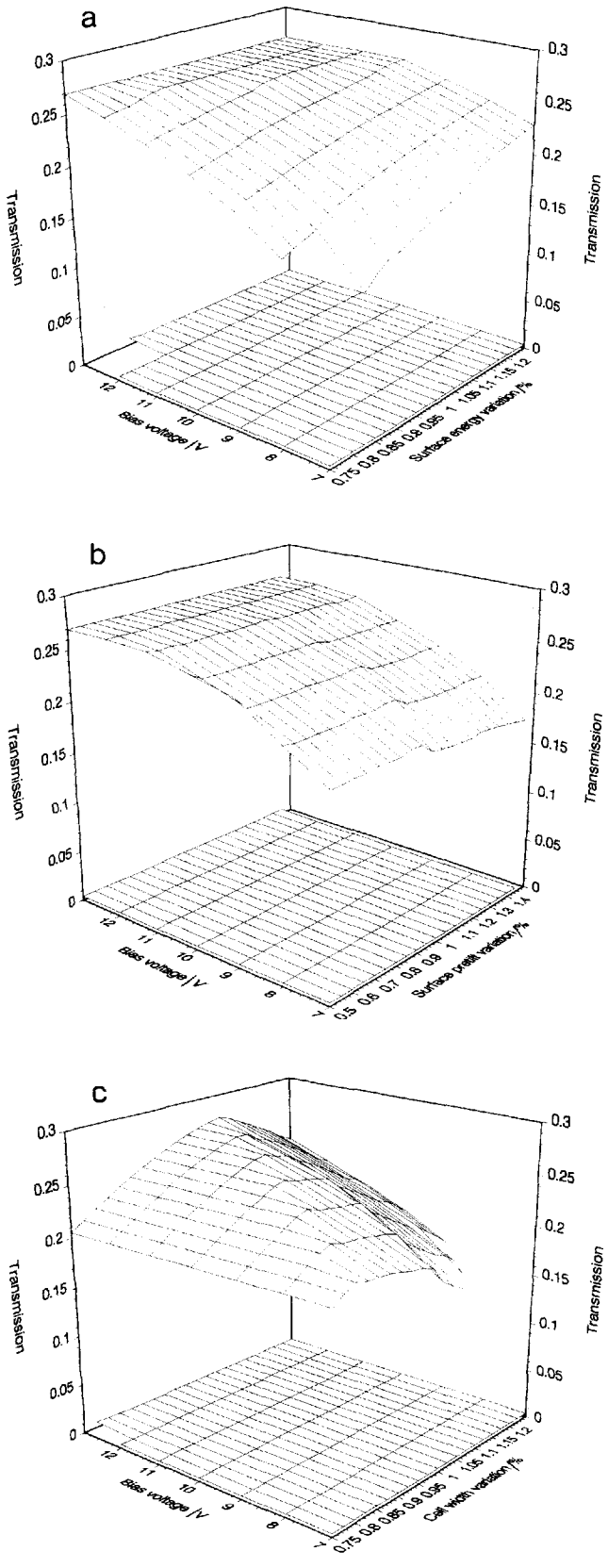

Figure 12. Optical transmission of the ferroelectric and antiferroelectric phases as a function of bias voltage and variation of the distributed parameter. (*a*) corresponds to surface energy variation, (*b*) to surface pretilt variation, and (*c*) to cell width variation.

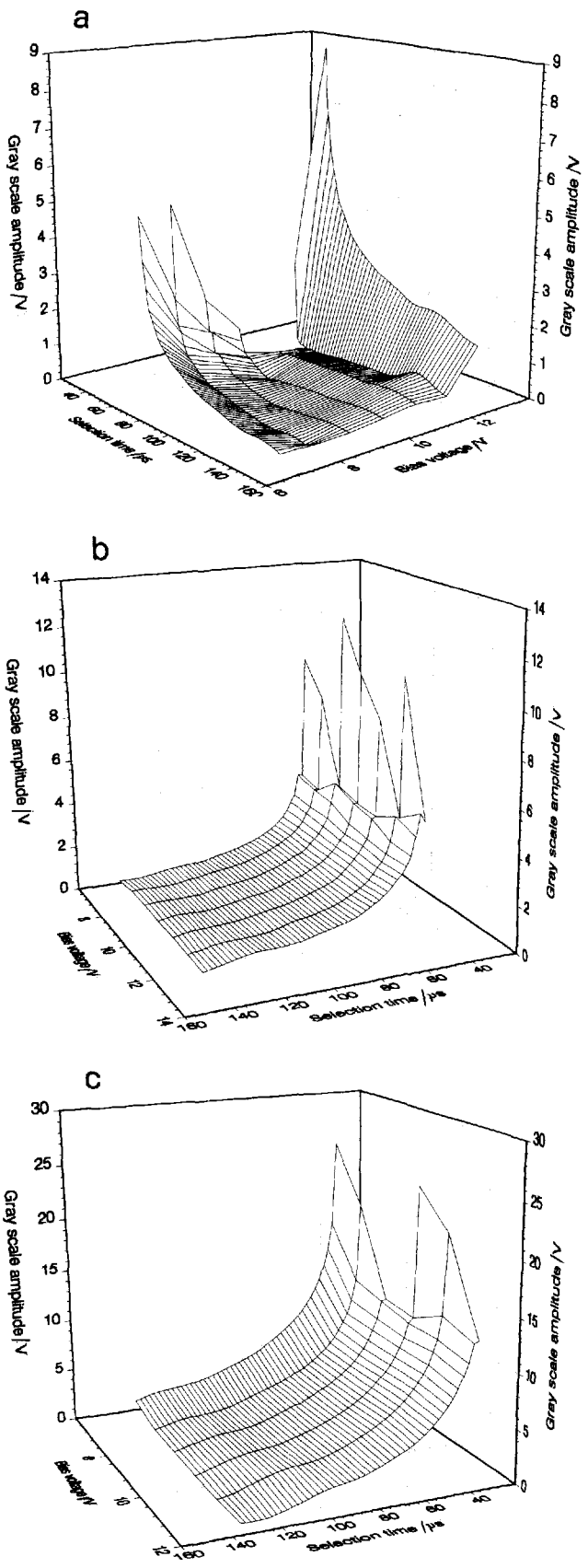

Figure 13. Voltage range of the greyscale as a function of selection time and bias voltage. The standard deviation of the distributed parameter is set to 3·5% of its central value. (*a*), (*b*) and (*c*) are the same as in figure 12 and its caption.

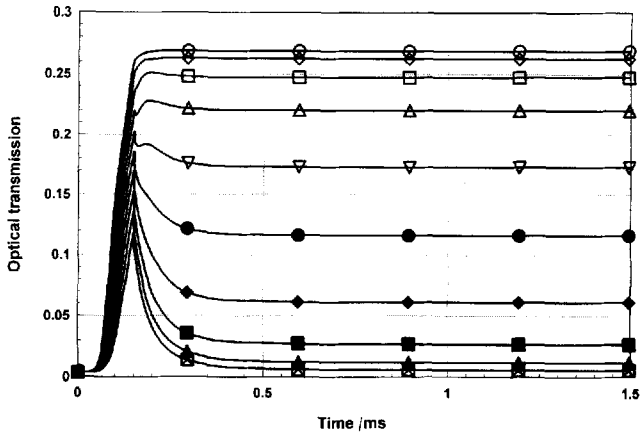

Figure 14. Temporal evolution of the optical transmission of an antiferroelectric liquid crystal cell driven by a waveform of the first type. Different selection voltages yield different stable transmission levels. Bias voltage is 10 V and selection time is 150 μs. The cell has its surface energy normally distributed. The surface energy standard deviation is 10% of its central value. Selection voltage/V: ⊠ 17·5, ▲ 18, ■ 18·5, ● 19, ◆ 19·5, ▽ 20, △ 20·5, ⊟ 21, ◇ 21·5, ○ 22.

4.3. *Dynamic greyscale calculation*

The model described in the previous paragraphs has been adapted for dynamic calculation of optical transmission in greyscale addressing. In this way, the optical response to a given voltage signal can be calculated and compared with experimental results.

Figure 14 is an example of the dynamic response of a pixel whose surface energy is normally distributed ($\sigma_\gamma = 10\%$). The bias voltage $V_b = 10$ V and the selection time $t_s = 150$ μs are kept constant, and the selection voltage is varied from 17·5 to 22·0 V. As seen in the figure, a full range of stable grey levels is obtained with these parameters.

The authors are indebted to Dr Masahiro Nakagawa for fruitful discussions. This work has been supported in part by ESPRIT III 8498 PROFELICITA Project and by the Spanish CICyT grant TIC 93-0638. JS wishes to thank CICyT for a research grant.

References

[1] ORIHARA, H., and ISHIBASHI, Y., 1991, *Ferroelectrics*, **122,** 177.
[2] YAMADA, Y., YAMAMOTO, N., MORI, K., KOSHOUBU, N., NAKAMURA, K., KAWAMURA, I., and SUZUKI, Y., 1993, *J. SID*, **1,** 289.
[3] NAKAGAWA, M., 1993, *Liq. Cryst.*, **14,** 1763.
[4] PAUWELS, H., DE MEYERE, A., and FORNIER, J., 1995, *Mol. Cryst. liq. Cryst.*, **263,** 469.
[5] OKADA, H., WATANABE, M., ONNAGAWA, H., and MIYASHITA, K., 1995, *Jpn. J. appl. Phys.*, **34,** L375.
[6] AKAHANE, T., and OBINATA, A., 1993, *Liq. Cryst.*, **15,** 883.